RSC Advances

ROYAL SOCIETY OF CHEMISTRY

www.rsc.org/advances

Journal Name

ARTICLE

Killing Cancer Cells by Delivering a Nanoreactor for Inhibition of Catalase and Catalytically Enhancing Intracellular Levels of ROS†

Received 00th January 20xx,
Accepted 00th January 20xx

DOI: 10.1039/x0xx00000x

www.rsc.org/

Ranjith Kumar Kankala,[a] Yaswanth Kuthati,[a] Chen-Lun Liu,[a] Chung-Yuan Mou[b] and Chia-Hung Lee[a*]

Intracellular hydrogen peroxide levels have the potential to be exploited in cancer therapy. We have synthesized uniform and size-controlled copper-impregnated mesoporous silica nanoparticles (Cu-MSN) containing a catalase inhibitor, 3-amino-1,2,4-triazole (AT) for ROS-mediated apoptosis in cancer cells. Copper species in the framework and aminotriazole loading were confirmed by electron spin resonance (ESR) and nuclear magnetic resonance (NMR) spectroscopies, respectively. The metal-ligand binding between the copper and AT are sensitive to the endosomal environment (pH-5.5) for the release of AT to inhibit cytosolic catalase activity. The subsequent enhanced level of intracellular hydrogen peroxide, after catalase inhibition, is transformed into toxic, reactive oxygen species (ROS) by the catalysis of Cu(II) on MSN. The intracellularly delivered Cu-MSN-AT exhibited significant activity against colon carcinoma (HT-29 cell line) substantiated by increased levels of ROS, where AT drove up the hydrogen peroxide concentration and also the level of free radicals through a Fenton-like reaction. The trigger of cell apoptosis was induced from ROS attack to lipid membranes in order for further radical propagation to cause lipid peroxidation and eventually, a decrease in the membrane fluidity and mitochondrial membrane potential. As a result, an increase in the membrane permeability caused the release of cytochrome c into the cytoplasm and further activation of apoptotic cascades to trigger DNA fragmentation. The design of the Cu-MSN-AT system takes advantage of a synergistic effect to inhibit antioxidant defenses and catalyze the activation of lethal ROS by the framework of copper ions to kill cancer cells which represents a novel chemotherapeutic strategy for ameliorating the toxic side effects from non-specific ROS generation in traditional chemotherapeutic agents.

Introduction

In the past decade, explosive growth of research into nanomaterials as drug delivery system has led to great advances in nanomedicine.[1] The rich varieties of nanoparticles suitable for use as drug carriers could increase the aqueous solubility of pharmaceuticals for improving the bioavailability and biocompatibility of drugs or protecting them from degradation.[2-5] Furthermore, these nanoparticles are advantageous because of their ability to target the site of action either by passive Enhanced Permeation and Retention (EPR) effect,[6] or by further conjugating various surface recognition groups for targeted drug release.[7-10] A step beyond this would be the delivery of nanoreactors such that the machinery could convert naturally available molecules in their surroundings to produce a therapeutic function.[11-14] Here, the goal is to deliver a catalytic action to a biological system such that naturally occurring molecules in malignant cells could be sabotaged in order to terminate them. In this work, we will demonstrate the ability of such nanoreactor carrying agents to divert the pathway of reactive oxygen species (ROS) in cancer cell so that active free radicals can be produced for killing the cancer cells.

Since ROS are naturally produced as a consequence of aerobic metabolism, cells have developed a variety of antioxidants to prevent the toxic accumulation of ROS. However, compared to normal cells, cancer cells often exhibit increased levels of intracellular ROS[15] and altered levels of antioxidant enzymes.[16] The resulting endogenous oxidative stress favours tumour growth by promoting genetic instability, cell proliferation and angiogenesis.[17] Although a negative impact shows that an increase of intrinsic ROS stress may induce cancer cells to transform into malignant types, further insults by generation of chemical ROS can cause lethal damages to cancer cells. A similar circumstance is observed during chemotherapy and radiotherapy through the overproduction of ROS to kill cancer cells to exhaust antioxidant defences.[18-20] To prevent oxidative damage from ROS, the malignant cancer cells show more dependency on antioxidant defences than normal cells. The enzyme catalase catalyses the decomposition of hydrogen peroxide into water and oxygen. It is one of the very important enzymes in protecting the cell from ROS damage. In this work,

[a] Department of Life Science and Institute of Biotechnology, National Dong Hwa University, Hualien, 974 (Taiwan).
[b] Department of Chemistry, National Taiwan University, Taipei 106 (Taiwan).
* Correspondence should be addressed- chlee016@mail.ndhu.edu.tw ;
Tel: +886-3-863-3-3677.

†Electronic Supplementary Information (ESI) available: [Dynamic light scattering (DLS)measurements, Powder X-Ray Diffraction curve, Fourier transform infrared (FT-IR) spectral curve, Thermogravimetric analysis curves, Drug release curve, Fluorescence spectrophotometric curves and Free radical determined by DCFDA Experimental methods section related to cell culture is also included]. See DOI: 10.1039/x0xx00000x

we designed a multi-functional nanoparticle system with which we inhibited the antioxidant enzyme (catalase) and generated exogenous ROS so as to cause the ROS-mediated cell apoptosis. Thus, cancer cells with increased oxidative stress are more likely to be vulnerable to damage by further ROS insults if the intracellular catalase can be inhibited.[21]

Our nanoreactor is based on mesoporous silica nanoparticles (MSN). Much research has been done since the discovery of mesoporous silica (MCM-41) which has highly ordered and adjusted pores from 2 nm to 30 nm with large surface area and rich surface functionalization capacity. Biocompatible MSNs have been used for a wide variety of applications in biomedicine,[22] such as intracellular imaging,[23] active targeting,[24] drug and gene delivery[25] and other applications. Because of their large internal surface area and volume, multifunctional MSNs can be easily built to obtain the combined effects of drug delivery and catalytic action. In a "double punch" design utilizing both the above functions, we would like first to inhibit the catalase to enhance the levels of hydrogen peroxide molecules and then catalytically convert them into hydroxyl radicals, thereby causing strong oxidative stress in the cancer cell.

For this purpose, MSNs are loaded with 3-amino-1,2,4-triazole (AT), an irreversible catalase inhibitor, for increasing the levels of hydrogen peroxide in cancer cells upon its intracellular release.[26] The MSNs will also carry copper ions that can eventually catalyze the conversion of H_2O_2 into hydroxyl radicals which will be responsible for anti-neoplasticity.[27, 28] We report on the synthesis of copper-impregnated MSNs (Cu-MSN) and AT-incorporated Cu-MSN (Cu-MSN-AT) samples to investigate the mechanism and efficiency of endocytosis of these nanoreactors along with the anti-cancerous activity in colon cancer (HT-29) cells.

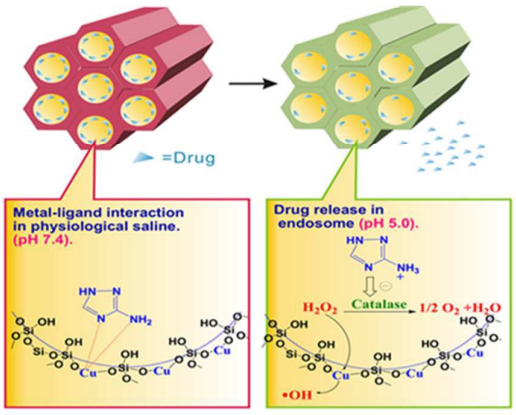

Fig. 1 Representation of Cu-MSN-AT framework and mechanistic illustration of delivery in a cancer cell environment.

The design concept of the Cu-MSN-AT is illustrated in Fig. 1. Copper (II) was loaded in the frameworks of MSNs. The aminotriazole (AT) molecules were also co-loaded in MSNs through both hydrogen bonding and coordination with Cu(II). The release of the protonated AT was initiated at a pH decrease (i.e., to 5.5) upon endocytosis. The coordinated unsaturated Cu(II) species were then available for catalysing a Fenton-like reaction to convert H_2O_2 into hydroxyl radicals. Increased intracellular levels of hydrogen peroxide were expected as a consequence of inhibition of the catalase upon release of AT.

Much research has been done into using MSN as drug carrier for controlled release,[29-37] targeting,[38] killing cancer cells,[39] overcoming drug resistance,[40, 41] and bio-imaging.[42-46] Gated approaches for controlled delivery[47, 48] of many anti-cancer moieties over various barriers have also been developed.[49-53] The previous approaches focus on delivery of some toxic external agents which can generate ROS or apoptosis cascades to further trigger programmed cell death.[54-60] Our work is a unique approach that mainly relies on the innate machinery of the cell to initiate the apoptosis pathway. Our nanoparticle system functions as a nanoreactor to subvert the intracellular ROS machinery to destroy the cancer cell, first by increasing the level of H_2O_2 and then by converting the H_2O_2 into highly toxic radicals.

Experimental Section

Materials

All the reagents, chemicals and organic solvents were of analytical grade at the highest purity, commercially available and were used without further purification. 3-amino-1,2,4-triazole (AT), copper nitrate trihydrate ($Cu(NO_3)_2 \cdot 3H_2O$), ethelenediaminetetraacetic acid (EDTA) were purchased from Alfa Aesar (a Johnson Matthey Company, Heysham, England). Triton X-100 was obtained from J.T. Baker Chemicals Pvt. Ltd. (Phillipsburg, NJ, U.S.A). Cetyltrimethylammonium bromide (CTAB), methanol, ammonium hydroxide (30%), 3-aminopropyltrimethoxysilane (APTS) and fluorescein isothiocyanate (FITC) and tetraethyl orthosilicate (TEOS) (98%) were obtained from Acros Organics Ltd. Sulforhodamine-B (SRB), hydrogen peroxide (H_2O_2), sodium phosphate dibasic (Na_2HPO_4), potassium phosphate monobasic (KH_2PO_4), citric acid, potassium phosphate dibasic (K_2HPO_4), Sodium hydroxide (NaOH), 2',7'-dichlorofluorescein diacetate (DCFDA), and formaldehyde (HCHO) were obtained from Sigma. Co. Ltd. (St. Louis, MO, U.S.A). Roswell Park Memorial Institute (RPMI)-1640 and Fetal bovine serum (FBS) were purchased from GIBCO/BRL Life Technologies (Grand Island, NY, U.S.A). Potassium bromide (KBr-FTIR grade) was obtained from Fisher Scientific Ltd. (Loughborough, U.K.). 4',6-Diamidino-2-phenylindole dihydrochloride (DAPI) and rhodium phalloidin were purchased from Invitrogen Ltd. (Eugene, Oregon, U.S.A). The comet assay kit was obtained from Trevigen (Trevigen,Inc. Helgerman court, Gaithersburg, MD U.S.A) and R&D systems (Minneapolis, MN, U.S.A) respectively. Western Kits including Sodium dodecyl sulfate poly acrylamide gel electrophoresis (SDS-PAGE), blotting/transfer kits and enhanced chemiluminescence (ECL) detection kits were obtained from Bio-Rad (U.S.A). The antibodies for Caspase-3, β-actin and the anti-mouse IgG horseradish peroxidase-conjugated secondary

antibody were purchased from Santa Cruz Biotechnology, U.S.A.

Physical Characterization

The structures of mesoporous silica materials were analyzed by powder X-ray diffraction (PXRD) with a Scintag X1 diffractometer using copper Kα radiation at λ =0.154 nm. FT-IR spectra were recorded on a Bruker Alpha spectrometer with a KBr pellet method using sample to KBr in 1: 300 ratio, pressed to form a thin film in a 7mm die and further subjected to analysis. The surface area, pore size, and pore volume were determined by N_2 adsorption–desorption isotherms obtained at 77 K on a Micrometric ASAP 2020 apparatus. The sample was outgassed at 10^{-3} Torr and 120 ºC for about 3 hours prior to the adsorption analysis. The pore size distribution curves were obtained from the analysis of the adsorption portion of the isotherms using the BJH (Barrett–Joyner–Halenda) method. The solid state ^{13}C CP/MAS NMR spectra were recorded operating at a 10-kHz spin rate and 100.62 MHz in a Bruker Avance III 400 NMR spectrometer from the Instrumentation Center at National Tsing Hua University, Taiwan. The particle size and its distribution were measured by dynamic light scattering (DLS) and ζ-potential using a Malvern Nano-HT Zetasizer. The samples were prepared by diluting the nanoparticle suspension with deionized water until the count rate was less than 1.5 Mcps (mega counts per second). The surface ζ-potential was obtained from an average of ten measurements. Thermogravimetric analysis (TGA) was performed on TGA Q50 V20, 13 Build 39 (Universal V4.5A TA Instruments). The temperature increased from ambient to 800 ºC at 20 ºC/min rate under dry nitrogen purge at a flow rate of 20 mL/min. EPR spectra were obtained at X-band using a Bruker EMX spectrometer equipped with a Bruker TE102 cavity. The microwave frequency was measured with a Hewlett-Packard 5246L electronic counter at 2 mW power and 4 G at 100 kHz modulation amplitude. Sample preparation was carried out by placing about 40 mg of the sample in a 4 mm quartz tube and observation was made at 77 K. TEM images were captured on a Hitachi H-7100 (Hitachi High Technologies Corporation, Tokyo, Japan) operating at 100 kV. Samples were prepared by dispersing nanoparticle ethanol solution deposited on carbon coated Cu grids and dried at RT. Centrifugation during the cell culturing process and nanomaterials synthesis was performed at an appropriate temperature using swing rotor Kubota KN-70 (Tokyo, Japan) and Hermle Z 36 HK (HERMLE Labortechnik GmbH, Wehingen, Germany) instruments, respectively. UV-Vis absorbance was recorded on a Genequant-1300 series spectrophotometer. Fluorescence images were captured using an Olympus microscope hybridized with DP73 color cameras. Fluorescence spectra were recorded using a Hitachi-F2700 fluorescence spectrophotometer equipped with Xenon lamp. HT-29 cell line was obtained from the Bioresource Collection and Research Center (Hsinchu, Taiwan). Fluorescence intensity and SRB absorbance were recorded using Perkin Elmer's EnSpire Multi-label plate reader (Santa Clara California, U.S.A). Flow cytometric quantification was performed using the BD Accuri C5 flow cytometer equipped with an FSC detection system and Argon Laser lamp (488 nm emission wavelength) while the data acquisition was in linear mode and visualized in logarithmic mode.

Synthesis of Cu-MSN

The Cu-MSN sample with hexagonal well-ordered pore structure was synthesized using tetraethoxysilane (TEOS), surfactant and a base catalyst in a two-step preparation.[61] The sol-gel process for the co-condensation of TEOS to synthesize Cu-MSN sample was as follows. First, CTAB (0.58 g) was dissolved in NH_4OH (0.51 M, 300 mL) at 40 ºC, and dilute TEOS (0.2 M in 5 mL ethanol) was added with vigorous stirring. After the solution was stirred for 4 hours, copper nitrate (43.9 mg in 5 mL ethanol) (Si/Cu -30) and TEOS (1.0 M in 5.0 mL of ethanol) were added with vigorous stirring for another 2 hours. Later, the solution was aged at 40 ºC for 24 hours and the nanoparticles were collected. Then, the nanoparticles were washed for several times using dd-H_2O and ethanol by centrifuging at 12,000 rpm for 18 minutes. Further, the surfactant templates were removed by extraction using ammonium nitrate in isopropanol (about 0.3 g of NH_4NO_3 in 50 mL of isopropanol stirred at 85 ºC for 24 hours).

Synthesis of Cu-MSN-AT Samples

Since the 3-amino-1,2,4-triazole (AT) molecule has a triazole structure, we impregnated the copper ion into the framework of MSN, which serves as an anchor essential for building up coordinated attractions to increase the drug loading efficiency and the preparation as follows. First, we prepared an AT stock solution with a concentration of 0.5 g AT in dd-H_2O (5 mL) adding 50 mg of Cu-MSN stirred overnight, and the UV absorbance of the supernatant was checked for loading efficiency. Finally the resultant was centrifuged and washed once with ethanol and re-suspended in dry ethanol for further studies to be performed. Similarly, FITC functionalized Cu-MSN (see ESI†) was also used to load AT and further cell studies were performed.

***In vitro* drug release study.**

Drug release study of the AT from MSN and Cu-MSN samples was performed. The nanohybrids (5 mg) were suspended in a phosphate buffer solution (pH-5.5 and 7.4) to simulate and mimic the release behaviour in endosomal pH and physiological fluid at 37 ºC while being rotated at 150 rpm. Aliquots were removed at regular intervals by centrifuging at 12,000 rpm for 10 minutes and the supernatant was analyzed by UV-Vis at a λmax of 289 nm. The study was continued by replacing the respective fresh simulated fluids at their corresponding time points. The released percentage of the drug in solution phase was determined by measuring the concentration periodically.

Results and discussion

From the TEM images shown in Fig. 2A and 2B, it is evident that the sizes of the MSNs are between 50 and 80 nm, which is optimum for cell internalization.[62] Hexagonally packed cylindrical nanochannels are clearly observed in the TEM image shown in Fig. 2B. Dynamic light scattering (DLS) measurements gave hydrodynamic diameters of MSN at 190 nm, Cu-MSN at 169 nm and Cu-MSN-AT at 320 nm, indicating a small extent of aggregation of the Cu-MSN-AT (Fig. S1). Nonetheless, they are still suspended well enough for cell-uptake. The mesostructures of Cu-MSN and Cu-MSN-AT were evidenced by X-ray diffraction (XRD) spectra, indicating hexagonal arrangements of the nanopores (Fig. S2), and confirming no structural degradation during the drug loading process. The Cu^{2+} ions were stable in the frameworks of MSN, as evidenced by the fact that the extracted MSN samples maintained the blue colour of typical Cu^{2+} ions (Fig. S2-b (inset)). Further, the loading of AT in the nanochannels of Cu-MSN showed the colour of the sample changed from blue to green, which resulted from the coordination of AT with Cu^{2+} ions (Fig. S2-c). Indeed, the triazoles and its derivatives have shown more diversity in coordination as ligands to transition metals such as copper and this chemistry was widely studied.[63] The binding affinity of triazole to copper is high enough and these complexes were also applied quite extensively in various fields.[64]

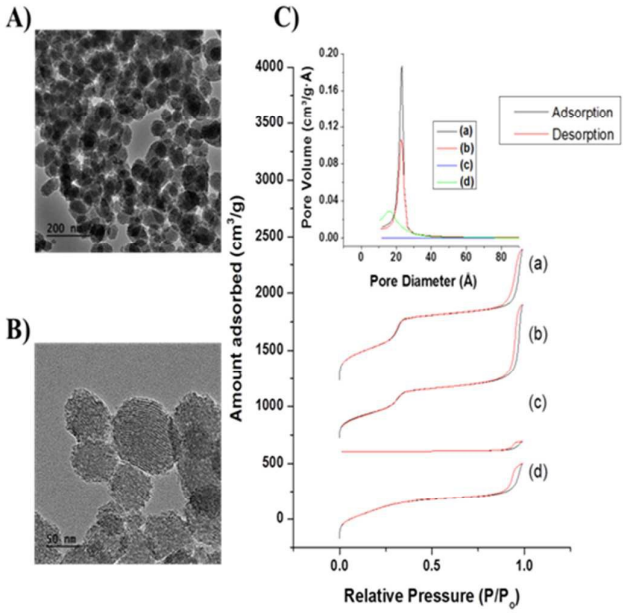

Fig. 2 TEM images of Cu-MSN viewed at various scales (A) 200 nm and (B) 50 nm. (C) BET curves of the respective modified samples (a) bare MSN, (b) Cu-MSN, (c) Cu-MSN-AT and (d) calcined sample of Cu-MSN-AT. Corresponding pore size distributions (inset Fig.).

Nitrogen adsorption-desorption isotherms and pore-size distribution of all the MSNs are shown in Fig. 2C. All the isotherms are in a type-IV gas adsorption isotherm based on IUPAC classification with no hysteresis loop. The BET surface area of the bare MSN was very high (i.e., 1586 m^2/g), with sharp distribution of pore diameter. This is possible because of the higher degree of extraction of CTAB in NH_4NO_3/isopropanol compared to extraction using ethanol (data not shown), which only gave a surface area of around 1000 m^2/g. Copper impregnated MSN gave a reduced surface area of 1189 m^2/g (Fig. 2C-b) because of the loading of Cu(II) in the framework and the textural properties of MSNs, which are summarized in Table S1. Nitrogen adsorption was dramatically reduced after loading the drug AT. The final BET surface area of Cu-MSN-AT was dropped to 20 m^2/g (Fig. 2C-c) because of heavy loading of the aminotriazole in Cu-MSN. The great reduction in pore volume from 1.86 to 0.15 cm^3/g provides further supportive evidence of its high loading of the drug. This was verified by calcination of the Cu-MSN-AT sample, after which it regained its original surface area (1084 m^2/g) and pore size (1.8 nm) (Fig. 2C-d). The ordered mesoporous structures were not disturbed during loading and calcination, which was also confirmed by FT-IR spectra (Fig. S3) and TGA (Fig. S4). These results also provided additional evidence that a large amount of AT molecules were indeed adsorbed in the nanochannels of Cu-MSN.

A FT-IR spectrum of the Cu-MSN was performed along with the successive modifications of it, and results were compared with the MSN (Fig. S3). It was observed that very negligible peaks of C-H stretch are present in the MSN samples, which are in accord with the weight loss in TGA (Fig. S4) representing that the surfactant template was extracted completely. For Cu-MSN-AT samples, the peaks at 1557, 1489 and 1365 cm^{-1} due to AT also confirmed high loading of AT (Fig. S3-c). In Table S1, textural and charge information about the nanoparticles are presented. At a pH of 6.0, the MSN exhibited a negative zeta potential around -22.9±0.2 mV, but it was less negative in the copper co-condensed MSN (Cu-MSN) (-9.5±0.1 mV), due to the positive charge of loaded copper ions. It seems the regain of zeta potential in the sample AT-loaded Cu-MSN-AT (-22.5±0.2 mV) indicated the AT were coordinated with Cu^{2+} ions. In addition, parts of the drug may favour the hydrogen bonding pattern of Si-$O^{\cdots}$HN between surface silanol and AT.

In addition, a lesser amount of weight loss was observed for bare MSN (Fig. S4-a) and Cu-MSN (Fig. S4-c). Cu-MSN-AT in TGA analysis shows aminotriazole degradation near 200 °C and 350 °C, which may be attributed to physical adsorption and coordination of AT, respectively (Fig. S4-d). The final loading percentage of the drug AT was estimated as 22% by weight of Cu-MSN, which is indeed very high. We attribute this high loading of AT to metal-ligand interactions with Cu(II) and AT. However, AT was loaded in bare MSN, which resulted in lesser amount (i.e., 5 % wt of MSN) due to physical adsorption (Fig. S4-b). Cu-MSN has another interesting feature in the release of AT after endocytosis. This release was relatively fast in the initial 2 hours and becoming constant rate over a longer term (Fig. S5). *In vitro* drug release of the AT in pH 5.5 (37%) was more than 7.4 (10%). This pH dependent behaviour is favourable for releasing the drug cargo in an endosomal environment. In this way, excess leakage of the drug in the

blood-stream before reaching the target site can be avoided. Similarly, the release of AT of bare MSN was performed, which resulted in the complete leach, irrespective to pH (Fig. S5).

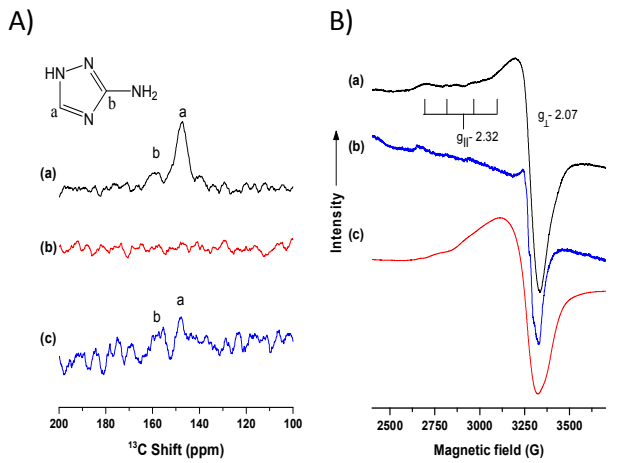

Fig. 3 A) Solid State (^{13}C) NMR spectra of (a) Aminotriazole (AT) loaded Cu-MSN, (b) spectrum of solids taken after release study of Cu-MSN-AT in PBS (pH-5.5) and (c) Physical mix of Cu-MSN and AT solids. B) ESR spectra of (a) Cu-MSN, (b) Cu-MSN-AT and (c) spectrum taken after release study of Cu-MSN-AT in PBS (pH-5.5).

Solid state NMR (^{13}C CP/MAS NMR spectroscopy) to characterize the aminotriazole conjugated copper-impregnated MSN (Cu-MSN-AT) and was clearly demonstrated the metal-drug coordination when compared with the physical mix (Cu-MSN as well as aminotriazole). The spectra (chemical shift) of the aminotriazole incorporated Cu-MSN resulted from the broadened peaks of node C and CH of the triazole ring in 3-amino-1,2,4-triazole at 158 and 147 ppm respectively (Fig. 3A-a). Nevertheless, the peaks of the sample i.e., physical mixing (Fig. 3A-c) were less intense. Further, the sensitivity of the coordination bond was verified in tumour pH, i.e., pH-5.5. The sample Cu-MSN-AT was subjected to release study in PBS (pH-5.5) and the spectra of the dried sample was recorded. Herewith, the peaks associated with the chemical shifts in Fig. 3A-a vanished confirming the sensitivity of the coordination bond between copper and aminotriazole at a tumour pH (Fig. 3A-b). Electron spin resonance (ESR) spectroscopy explored the structural characteristics of the Cu(II)-impregnated mesoporous silica nanoparticles. The spectra displayed an anisotropic copper (II) signal at 77 K (Fig. 3B-a). The g values were calculated using the usual methods and are in agreement with the previous reports.[65] This reveals that the copper (II) centered systems were axial coordinated with siloxyl groups, and the $g_{\|}$ (2.32) > $g_{\perp}$ (2.07) > 2.02 suggests the copper (II) in the framework had a distorted square pyramidal octahedral coordination within siliceous framework due to the Jahn-Teller effect.[66] After aminotriazole conjugation the copper (II) intensity was decreased, because it was converted to copper (I) due to charge transfer. When the same sample was exposed to a PBS buffer (pH-5.5) to cleave the sensitive coordination linkage, a regain of the copper (II) species in the MSN framework was observed with slight change in g value compared to Cu-MSN. As a consequence, spectroscopic studies of Cu-MSN indicate clearly that copper (II) complex was formed in the MSN matrix.

A plausible mechanism in cancer therapy using aminotriazole conjugated in copper co-condensed MSN is represented in Fig. 4. When the Cu-MSN-AT nanoparticles were delivered into the tumour tissues, the nanoparticles were uptaken by the cancer cells through endocytosis. The acidic pH of endosomes (or lysosome) may trigger the AT release through the protonation of nitrogen atoms and weakening of the metal-ligand coordination bonds.[67] Thus, the released AT molecules may escape from endosomes and inhibit the cytosolic catalase activity. For this approach, we can increase the intracellular hydrogen peroxide concentration and further catalyse by the framework Cu^{2+} ions to produce cytotoxic free radicals by the reactions shown in equation (1)-(2). The Cu^{2+} ions of MSN framework reacted with H_2O_2 to generate Cu^{+} and hydroperoxyl radicals by equation (1). The hydroxyl radicals were further produced by Fenton-like reaction (equation (2)).[27] The ROS generation in cancer cells caused the lipid peroxidation; eventually a decrease in the membrane fluidity and mitochondrial membrane potential occurs. The resulted increase in the mitochondrial membrane permeability may further induce the release of cytochrome c into the cytoplasm and activation of apoptotic cascades to trigger DNA fragmentation.

$$Cu^{2+}\text{-MSN} + H_2O_2 \rightarrow Cu^{+}\text{-MSN} + HO_2\cdot + H^{+} \quad (1)$$
$$Cu^{+}\text{-MSN} + H_2O_2 \rightarrow Cu^{2+}\text{-MSN} + OH^{-} + OH\cdot \quad (2)$$

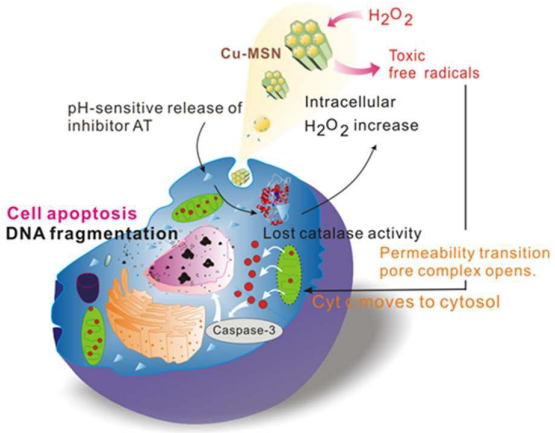

Fig. 4 Representation of nanocontainer internalization into the cell and the plausible mechanism that subsequently leads to cell apoptosis because of free radical generation.

Anti-proliferative screening of aminotriazole immobilized Cu-MSN was evaluated by sulforhodamine B colorimetric assay based on the principle of measuring total cellular protein content. This is preferred over other assay methods like MTT showing wider linear range with cell number.[68] The IC_{50} of the

respective samples were calculated and the plots were in accord with respective increasing concentrations, as shown in the Fig. 5. Cu-MSN is mildly toxic because of intrinsic ROS stress with largely endogenous H_2O_2 expression in cancer cells. Nevertheless, AT-loaded Cu-MSN is approximately 20 fold more noxious than the Cu-MSN control (IC_{50} in Fig. 5) and 15 fold more than MSN-AT (IC_{50} in Fig. S6b). Biocompatibility of various MSN samples was performed using normal fibroblast (3T3) cell line and the consequences were elucidated in Fig. S7. We observed bare MSN resulted in more viable cells at 500 µg/mL, however remaining samples (MSN-AT, Cu-MSN and Cu-MSN-AT) exhibited toxicity at and more than 125 µg/mL. The cytotoxicity in normal fibroblast cells is lesser compared to the cancer (HT-29) cell line, because of abridged uptake.[15]

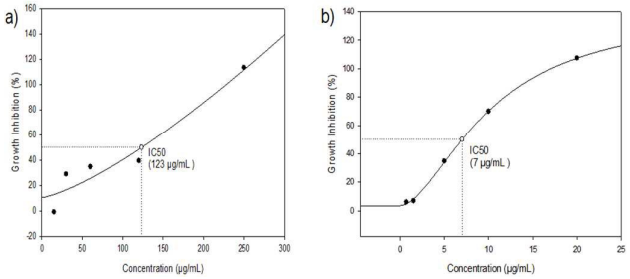

Fig. 5 Cell growth inhibition from the SRB assay of (a) Cu-MSN and (b) Cu-MSN-AT complexes to HT-29 cells. Various concentrations of Cu-MSN-AT complexes were added to cells. Then, cells were fixed after 24 hours, stained with SRB, washed with dd-H_2O, and subsequently solubilized before absorbance was read at a wavelength of 515 nm. IC_{50} was determined from the graphs.

The successful conjugation of FITC in the framework of MSN without any leaching was confirmed by the green fluorescent of the FITC-Cu-MSN and FITC-Cu-MSN-AT suspension (Fig. S8b and S6c) and absence of fluorescence in the supernatant of the centrifuged samples (Fig. S8b' and S8c'). Also the positive charge functionalities (copper) on the Cu-MSN-AT could elevate the cell internalization of particle with more ease. The nanosized particles explored via the maximum uptake by endocytosis and MSN are non-toxic at a dose level of 100 µg/mL, when not carrying any drug. As shown in Fig. 6, the images of fluorescence microscopy from FITC-Cu-MSN (Fig. 6a) and FITC-Cu-MSN-AT (Fig. 6b) nanoparticles treated with HT-29 cancer cells displayed the effective delivery of nanoparticles into the cells. In addition, some characteristic morphology was associated with cell apoptosis, such as chromatin condensation and cell shrinking.

The cellular uptake was further estimated by flow cytometry (Fig. 7-left). The shift of cell population to the high fluorescent intensity indicated that the FITC-Cu-MSN sample had higher cellular uptake at 4 hours treatment. The quantification of intracellular ROS production from green fluorescence of the treated cell was also monitored by flow cytometry (Fig. 7-right). Aminotriazole induced ROS generation was determined by measurement of the fluorescence intensity of DCF, which was produced from DCFH rapid oxidation by intracellular ROS. The results were compared with the ROS generated by adding hydrogen peroxide (1 mM) as a positive control. The cell population had shifted to a high DCF fluorescent intensity, which indicated the generation of high ROS production may further affect to cells due to oxidative damage to DNA, protein and lipid membranes.[69]

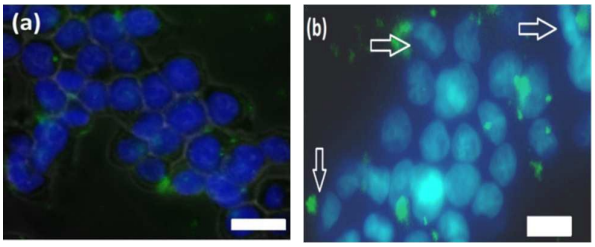

Fig. 6 (a) Fluorescent images captured during cell uptake study using FITC-Cu-MSN (100 µg/mL) in HT-29 cell line merged with bright field image (scale bar- 20 µm) and (b) fluorescent images captured for representation of nucleus shrinkage (indicated with arrows) stained using DAPI when treated with FITC-Cu-MSN-AT (60 µg/mL) in HT-29 cell line (scale bar- 10 µm).

Fluorescence emitted by DCF was also captured with a microscope (Fig. 8A) which reflects that the visual observation of ROS generated in treated cells (Fig. 8A-c and d) is comparable to hydrogen peroxide (Fig. 8A-b), which is significantly different from the control, as shown in Fig. 8A-a. A quantitative ROS concentration was determined by measurement of the fluorescent intensity of dichlorofluorescein (DCF) in a multi-detection microplate reader. The generation of ROS levels from Cu-MSN-AT showed a concentration-dependent manner (Fig. S9). The slight increase of intracellular ROS under the high concentration of Cu-MSN treatment may come from the catalysis of the endogenous H_2O_2 in the cancer cell. Single cell gel electrophoresis (comet assay) was performed for investigating the DNA fragmentation by Cu-MSN-AT (Fig. 8B). The comet assay was carried out by placing the HT-29 cells and agarose gel on a microscope slide. Further treatment with detergents and high ionic strength salts can release chromatin under an alkaline electrophoresis condition. The comet assay has a very high sensitivity, which can be used to detect various DNA damages such as single- and double- strand DNA breaks.[70] The results were obtained using further staining with a fluorescent dye (SYBR Green) to reveal a comet with head and tail. The long tail in Fig. 8B-b represents the cleaved DNA resultant of the apoptosis in the cell. Fluorescence images for comparison of both controls possessed compact DNA around 7-9 µm (Fig. 8B-a) and treated with Cu-MSN-AT in which the DNA has shown an elongation measuring around 35 µm (Fig. 8B-b). The possible mechanisms for inducing DNA damage may come from (1) lethal free radicals attacking DNA as a result of the synergistic effect of inhibiting antioxidant defences and catalytic reactions of Cu-MSN nanoreactor and (2) triggering of apoptotic cascades by stimulating the activation of a family of proteases called caspases.

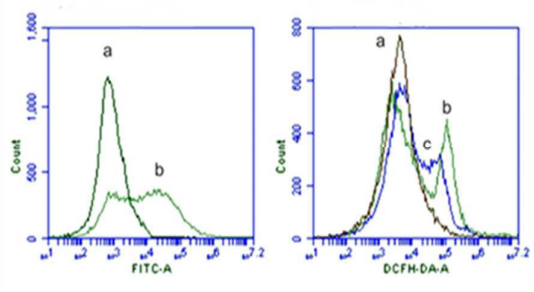

Fig. 7 Flow cytometric analyses of (1) on the left: cell uptake of FITC conjugated Cu-MSN (a) control and (b) treated for 4 hours with FITC-Cu-MSN (100 µg/mL), (2) on the right: increased production of DCF-DA fluorescence with cells treated with (a) control, (b) Cu-MSN-AT (60 µg/mL) and (c) hydrogen peroxide (1mM).

Results of free radical-mediated lipid peroxidation of HT-29 cancer cell by aminotriazole loaded Cu-MSN are presented in the Thiobarbituric acid reactive substances (TBARS) assay (Fig. 9). Lipid peroxidation products were resulted from the reaction of membrane lipids of polyunsaturated fatty acids and different free radicals from ROS. This can lead to alteration of the structure and function of cell membranes and further cause cell injury and cell death. TBARS were formed in which a by-product of lipid peroxidation malondialdehyde (MDA) was quantified by red fluorescent TBA adducts.

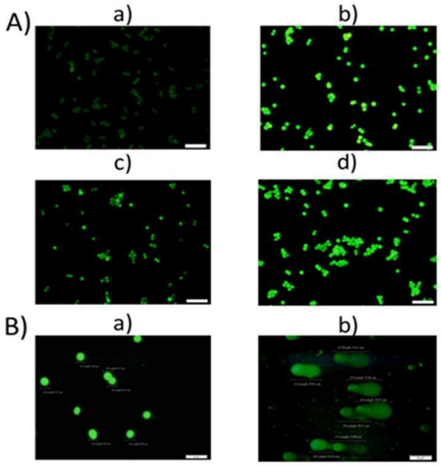

Fig. 8 (A) ROS determination measured by intensity of dichlorofluorescein (DCF) fluorescence. Images captured by fluorescent microscope of HT-29 cell line, after incubation with DCF-DA with respective concentrations (a) control, (b) positive control (1 mM Hydrogen peroxide (H_2O_2)) (c) Cu-MSN-AT (15 µg/mL) and (d) Cu-MSN-AT (60 µg/mL). (B) Induced DNA fragmentation was detected by single cell gel electrophoresis (comet assay); (a) cells treated without (control), (b) Cu-MSN-AT (60 µg/mL) (treatment)and incubated for 24 hours. Nucleic acid was stained with SYBR green.

We observed some partial lipid peroxidation with Cu-MSN, because of the high ROS stress of non-radical molecules such as hydrogen peroxide in cancer cells; but much more lipid peroxidation was detected with Cu-MSN-AT, which is concentration dependent and comparable to the positive control, diethyl maleate (DEM).[71] The catalase inhibitor, aminotriazole, enhances the generation of free radicals for initiation of lipid peroxidation. Once lipid peroxidation is stimulated, the derivatives of organic radicals may lead to a propagation of the peroxidation reaction and result in substantial cell damage. In addition, lipid peroxidation may decrease the lipid fluidity, but increase the membrane permeability. Therefore, many of the free radicals were generated after the treatment of the Cu-MSN-AT nanoparticles which may damage the mitochondrial membranes and thereby cause the release of cytochrome c and activation of the apoptotic pathway.

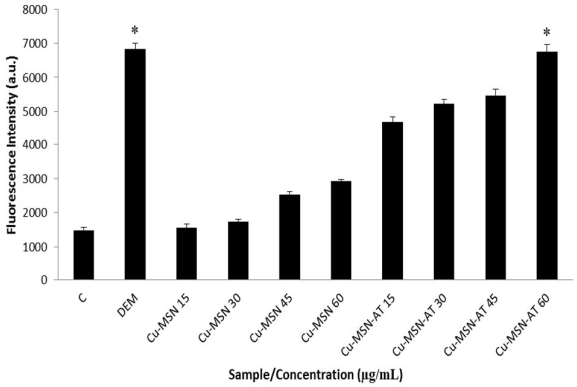

Fig. 9 Lipid peroxidation by TBARS assay of various concentrations of Cu-MSN, Cu-MSN-AT along with negative (PBS) and positive control (10 mM DEM) in HT-29 cell line and the absorbance monitored at (Ex/Em = 532/553 nm) *represents $p<0.001$ (one way ANOVA using a Tukey test).

Intracellular hydrogen peroxide levels were reduced because of the enzymatic degradation by catalase in intracellular peroxisome, and inhibition of this enzyme leads to rises in levels of hydrogen peroxide in the cells and eventually, rises in hydroxyl radical levels through a Fenton-type reaction. Catalase enzyme inhibition by aminotriazole was due to irreversible catalase binding with AT. Measurement of loss of absorbance of H_2O_2 by UV (at 240 nm) can be correlated to the amount of catalase activity by aminotriazole,[72] which shows a loss of catalase activity of increasing concentration at a higher significance rate around 100 µg/mL of Cu-MSN-AT by 80% of the control as presented in Fig. 10.

A foam test was also performed to show that catalase activity was blocked by aminotriazole being released from the nanoreactor (Fig. S10). The foam was generated from the conversion of hydrogen peroxide into water and oxygen by catalase catalysis; therefore, the bubbles were filled with this oxygen. The more bubbles generated, the higher the catalase activity inside the cells. After the successful uptake of Cu-MSN-AT nanoparticles (15 and 60 µg/mL) by the HT-29 cell line, the efficacy in inhibition of enzyme catalase was observed with the reduction in the amount of foam compared to the control. The

measured values determine the catalase status in the cell after exposure to hydrogen peroxide to catalyze it, and show it was reduced significantly by 90% of the control in Cu-MSN-AT-60 treated cells.

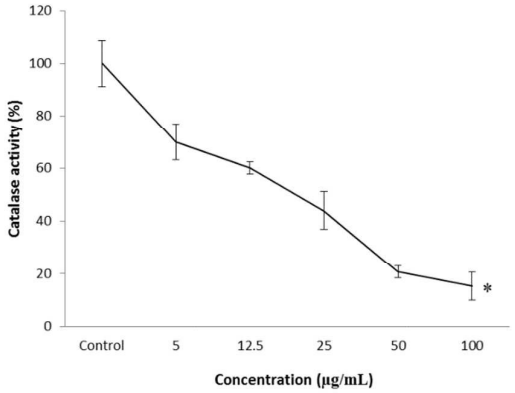

Fig. 10 Intracellular hydrogen peroxide levels in HT-29 cells treated with different concentrations of Cu-MSN-AT for 24 hours. *represents p<0.001 for all the concentrations (one way ANOVA using a Tukey test)

In many cells, apoptosis is associated with the loss of the mitochondrial membrane potential (MMP), which is a limiting factor in the apoptotic pathway. Reduction of MMP is among the changes encountered during the early stage of apoptosis. Jing *et al.* have reported that arsenic trioxide (ATO) can inhibit the glutathione peroxidase and increase the intracellular hydrogen peroxide concentration which leads to a decrease of MMP, release of cytochrome c, and caspase activation.[73] Mitochondrial membrane potential loss detection during cell apoptosis was determined using vital cationic carbocyanine dye, JC-1, a sensitive marker for misappropriation of mitochondrial function. Cell death in apoptosis can be perceived by the green fluorescence.[74] In healthy cells, the J-aggregates resulted due to hyperpolarized state of mitochondrial membrane i.e., red in colour as represented in Fig. 11A (control cell). With increasing the dose of Cu-MSN-AT to 30 and 60 μg/mL, the green fluorescence of the JC-1 marker gradually appears indicating the apoptosis pathway. As for the quantitative ratios, we observed the reduced MMP with increasing concentration of Cu-MSN-AT (Fig. 11B). The treated cells underwent programmed destruction, i.e. disappearance of J-aggregates because the mitochondria lipid membranes were attacked by the intracellular ROS. The loss of the MMP may decrease electrostatic attractions between cytochrome c and the mitochondria intermembrane; therefore, the cytochrome c was further released into the cytoplasm to activate apoptosis cascades for further DNA fragmentation and cell apoptosis. Thus, the lethal ROS can cause cell apoptosis through the lipid peroxidation, alteration in mitochondrial transmembrane potential and increase of mitochondria membrane permeability which results in cytochrome c release into the cytoplasm, and triggers caspase 3 activation.

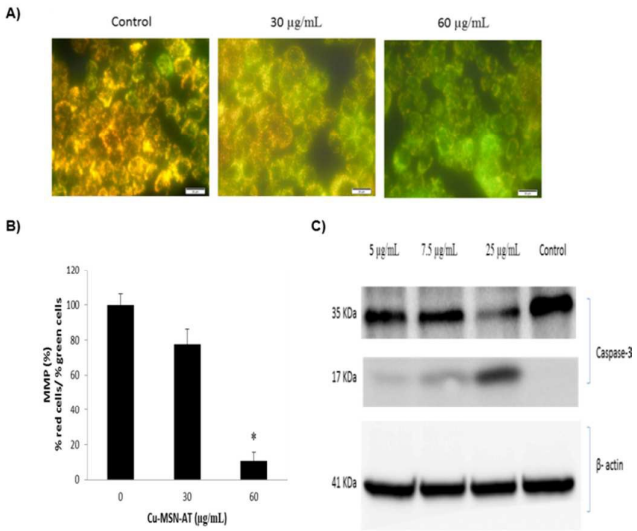

Fig. 11 A) Fluorescent images of mitochondria membrane potential (MMP) using JC-1 dye incubated for 30 minutes in HT-29 cell line after 24 h of treatment with respective concentrations. **B)** Graphical representation of % MMP calculated (% red cells/ % green cells). **C)** Induction of apoptosis in HT-29 cell line by Cu-MSN-AT, without treating the cells (control) and with various concentrations of Cu-MSN-AT complexes for 24 h. Cells were lysed for the determination of caspase-3 cleavage and β-actin protein using the western blot method. * represents p<0.001 (one way ANOVA using a Tukey test)

In the sequence of nuclear condensation and DNA fragmentation, apoptosis associated proteolysis leads to cell destruction mainly due to one of the executioner caspases (caspase-3) of apoptosis. Since generation of the caspase family of proteins occurs by pro-apoptotic signals.[75] Western blotting was performed for the observation of caspase-3 fragmenting at 17 KDa as shown in Fig. 11C and confirms that the cell underwent apoptosis rather than necrosis. The dose-dependent cleavage of caspase-3 confirms intrinsic (mitochondrial) pathways for apoptosis after the release of AT and the increase of ROS. Caspase-3 generated is also responsible for the DNA fragmentation and eventual nuclear shrinkage is observed. We have demonstrated a strategy of killing cancer cells through promoting free radical generation through the delivery of a nanoreactor Cu-MSN-AT. The action relies on the intrinsic higher level of ROS in cancer cells and its further amplification through the action of this well-designed nanoreactor. Two built-in features will help it to effectively kill the cancer cells: (1) the release of aminotriazole at low pH leads to intracellular delivery after endocytosis. (2) The higher H_2O_2 levels in the cancer cells would also give rise to increased generation of hydroxyl radicals by the catalysis of the Cu-MSN nanoreactor. Thus, reactive oxygen species may directly induce most apoptosis in cancer drug therapy; our strategy of amplifying ROS to produce even more toxic hydroxyl radical may be used in a co-delivery with other cancer drugs since the

larger pore volume in MSN can be easily used in a cocktail co-delivery approach.

Conclusions

We have presented a system of copper-impregnated mesoporous silica nanoparticles for pH-sensitive release of the catalase inhibitor (AT) at the endosomal pH through metal affinity interactions. Copper (II) species incorporated in the frameworks of MSN and aminotriazole coordination to the copper were confirmed by electron spin resonance (ESR) and nuclear magnetic resonance (NMR) spectroscopies, respectively. The intracellular pH-sensitive release of AT to increase levels of H_2O_2 concentration, which was in turn catalysed by Cu(II) through a Fenton-like reaction to generate lethal ROS. The mechanism of ROS in triggering apoptosis of cancer cells is thought to be associated with the lipid peroxidation from ROS attack. For the initiation of ROS production, lipid membranes reacted to produce organic radicals, which on further reacts through radical propagation to derive the end products of reactive aldehydes of malondialdehyde (MDA). In the course of lipid peroxidation reaction, the mitochondrial membranes were damaged greatly, as evidenced by reduction in both fluidity and mitochondrial membrane potential. However, a relative increase in the membrane permeability may cause the release of mitochondrial cytochrome c from the mitochondria intermembrane space into the cytoplasm which can activate apoptotic cascades (caspase-3) causing further DNA fragmentation and cell apoptosis. Thus, a highly efficient ROS generation through synergistic inhibition of antioxidant defences by a catalytic Cu-MSN nanoreactor could provide a novel therapeutic strategy to kill cancer cells. The use of the Cu-MSN-AT system takes advantage of the high levels of free radical propagation in cancer cells, and may not only augment traditional chemotherapy, but also provide an opportunity to develop novel anticancer strategies.

Acknowledgements

We are thankful to the Ministry of Science and Technology, Taiwan for a research grant (NSC 101-2113-M-259-003-MY2, MOST 103-2113-M-259-005-MY2). We wish to thank Prof. Shyue-Chu Ke of the Department of Physics, National Dong Hwa University for assisting with the ESR measurements.

References

1. A. G. Cuenca, H. B. Jiang, S. N. Hochwald, M. Delano, W. G. Cance and S. R. Grobmyer, *Cancer*, 2006, 107, 459-466.
2. Y. Z. Zhang, J. C. Wang, X. Y. Bai, T. Y. Jiang, Q. Zhang and S. L. Wang, *Mol. Pharm.*, 2012, 9, 505-513.
3. M. H. Kim, H. K. Na, Y. K. Kim, S. R. Ryoo, H. S. Cho, K. E. Lee, H. Jeon, R. Ryoo and D. H. Min, *ACS Nano*, 2011, 5, 3568-3576.
4. J. Mendez, M. M. Cruz, Y. Delgado, C. M. Figueroa, E. A. Orellano, M. Morales, A. Monteagudo and K. Griebenow, *Mol. Pharm.*, 2014, 11, 102-111.
5. Y. Chen, H. R. Chen and J. L. Shi, *Mol. Pharm.*, 2014, 11, 2495-2510.
6. H. L. Kim, S. B. Lee, H. J. Jeong and D. W. Kim, *RSC Adv.*, 2014, 4, 31318-31322.
7. J. M. Rosenholm, C. Sahlgren and M. Linden, *Nanoscale*, 2010, 2, 1870-1883.
8. L. M. Pan, Q. J. He, J. N. Liu, Y. Chen, M. Ma, L. L. Zhang and J. L. Shi, *J. Am. Chem. Soc.*, 2012, 134, 5722-5725.
9. C. E. Ashley, E. C. Carnes, K. E. Epler, D. P. Padilla, G. K. Phillips, R. E. Castillo, D. C. Wilkinson, B. S. Wilkinson, C. A. Burgard, R. M. Kalinich, J. L. Townson, B. Chackerian, C. L. Willman, D. S. Peabody, W. Wharton and C. J. Brinker, *ACS Nano*, 2012, 6, 2174-2188.
10. S. Y. Tan, C. Y. Ang, P. Z. Li, Q. M. Yap and Y. L. Zhao, *Chem.-Eur. J.*, 2014, 20, 11276-11282.
11. F. P. Chang, Y. P. Chen and C. Y. Mou, *Small*, 2014, 10, 4785-4795.
12. F. P. Chang, Y. Hung, J. H. Chang, C. H. Lin and C. Y. Mou, *ACS Appl. Mater. Interfaces*, 2014, 6, 6883-6890.
13. H. Chen, W. He and Z. Guo, *Chemical Communications*, 2014, 50, 9714-9717.
14. X. L. Fang, X. J. Zhao, W. J. Fang, C. Chen and N. F. Zheng, *Nanoscale*, 2013, 5, 2205-2218.
15. R. K. Kankala, Y. Kuthati, C.-L. Liu and C.-H. Lee, *RSC Advances*, 2015, 5, 42666-42680.
16. J. Watson, *Open Biology*, 2013, 3.
17. H. Pelicano, D. Carney and P. Huang, *Drug Resistance Updates*, 2004, 7, 97-110.
18. A. Miyajima, J. Nakashima, K. Yoshioka, M. Tachibana, H. Tazaki and M. Murai, *British Journal of Cancer*, 1997, 76, 206-210.
19. Q. Kong and K. O. Lillehei, *Medical Hypotheses*, 1998, 51, 405-409.

20. X. Y. Li, Q. J. He and J. L. Shi, *ACS Nano*, 2014, 8, 1309-1320.
21. J. M. Mates and F. M. Sanchez-Jimenez, *Int J. Biochem. Cell Biol.*, 2000, 32, 157-170.
22. I. I. Slowing, B. G. Trewyn, S. Giri and V. S. Y. Lin, *Adv. Funct. Mater.*, 2007, 17, 1225-1236.
23. J. Kim, H. S. Kim, N. Lee, T. Kim, H. Kim, T. Yu, I. C. Song, W. K. Moon and T. Hyeon, *Angew. Chem.-Int. Edit.*, 2008, 47, 8438-8441.
24. R. Wittig, J. M. Rosenholm, E. von Haartman, J. Hemming, F. Genze, L. Bergman, T. Simmet, M. Linden and C. Sahlgren, *Nanomedicine*, 2014, 9, 971-987.
25. Y. Zhang, Z. Y. Hu, G. J. Xu, C. Z. Gao, R. A. Wu and H. F. Zou, *Nano Res.*, 2014, 7, 1103-1115.
26. E. Margoliash, A. Novogrodsky and A. Schejter, *The Biochemical journal*, 1960, 74, 339-348.
27. L. Norena-Franco, I. Hernandez-Perez, P. Aguilar and A. Maubert-Franco, *Catalysis Today*, 2002, 75, 189-195.
28. J. Fang, T. Seki and H. Maeda, *Advanced drug delivery reviews*, 2009, 61, 290-302.
29. A. Baeza, M. Colilla and M. Vallet-Regi, *Expert Opin. Drug Deliv.*, 2015, 12, 319-337.
30. J. L. Vivero-Escoto, Slowing, II, B. G. Trewyn and V. S. Y. Lin, *Small*, 2010, 6, 1952-1967.
31. J. Lee, H. Kim, S. Han, E. Hong, K. H. Lee and C. Kim, *J. Am. Chem. Soc.*, 2014, 136, 12880-12883.
32. S. R. Choi, D. J. Jang, S. Kim, S. An, J. Lee, E. Oh and J. Kim, *J. Mat. Chem. B*, 2014, 2, 616-619.
33. S. H. Cheng, W. N. Liao, L. M. Chen and C. H. Lee, *J. Mater. Chem.*, 2011, 21, 7130-7137.
34. T. M. Guardado-Alvarez, L. S. Devi, M. M. Russell, B. J. Schwartz and J. I. Zink, *J. Am. Chem. Soc.*, 2013, 135, 14000-14003.
35. L. Mondragon, N. Mas, V. Ferragud, C. de la Torre, A. Agostini, R. Martinez-Manez, F. Sancenon, P. Amoros, E. Perez-Paya and M. Orzaez, *Chem.-Eur. J.*, 2014, 20, 5271-5281.
36. Q. L. Li, Y. F. Sun, Y. L. Sun, J. J. Wen, Y. Zhou, Q. M. Bing, L. D. Isaacs, Y. H. Jin, H. Gao and Y. W. Yang, *Chem. Mat.*, 2014, 26, 6418-6431.
37. P. Zhang, T. Wu and J. L. Kong, *ACS Appl. Mater. Interfaces*, 2014, 6, 17446-17453.
38. L. M. Pan, J. N. Liu, Q. J. He and J. L. Shi, *Adv. Mater.*, 2014, 26, 6742-6748.
39. L. Feng, K. Li, X. Shi, M. Gao, J. Liu and Z. Liu, *Advanced Healthcare Materials*, 2014, 3, 1261-1271.
40. X. X. Zhang, F. F. Li, S. Y. Guo, X. Chen, X. L. Wang, J. Li and Y. Gan, *Biomaterials*, 2014, 35, 3650-3665.
41. L. M. Pan, J. A. Liu, Q. J. He, L. J. Wang and J. L. Shi, *Biomaterials*, 2013, 34, 2719-2730.
42. Y. Wang and H. C. Gu, *Adv. Mater.*, 2015, 27, 576-585.
43. F. Chen, T. R. Nayak, S. Goel, H. F. Valdovinos, H. Hong, C. P. Theuer, T. E. Barnhart and W. B. Cai, *Mol. Pharm.*, 2014, 11, 4007-4014.
44. W. P. Fan, B. Shen, W. B. Bu, F. Chen, Q. J. He, K. L. Zhao, S. J. Zhang, L. P. Zhou, W. J. Peng, Q. F. Xiao, D. L. Ni, J. N. Liu and J. L. Shi, *Biomaterials*, 2014, 35, 8992-9002.
45. S. B. Lee, H. L. Kim, H. J. Jeong, S. T. Lim, M. H. Sohn and D. W. Kim, *Angew. Chem.-Int. Edit.*, 2013, 52, 10549-10552.
46. J. A. Liu, W. B. Bu, S. J. Zhang, F. Chen, H. Y. Xing, L. M. Pan, L. P. Zhou, W. J. Peng and J. L. Shi, *Chem.-Eur. J.*, 2012, 18, 2335-2341.
47. Q. Gan, X. Y. Lu, W. J. Dong, Y. Yuan, J. C. Qian, Y. S. Li, J. L. Shi and C. S. Liu, *J. Mater. Chem.*, 2012, 22, 15960-15968.
48. Y. N. Zhao, J. L. Vivero-Escoto, Slowing, II, B. C. Trewyn and V. S. Y. Lin, *Expert Opin. Drug Deliv.*, 2010, 7, 1013-1029.
49. J. K. Fu, Y. C. Zhu and Y. Zhao, *J. Mat. Chem. B*, 2014, 2, 3538-3548.
50. Q. Zhang, K. G. Neoh, L. Q. Xu, S. J. Lu, E. T. Kang, R. Mahendran and E. Chiong, *Langmuir*, 2014, 30, 6151-6161.
51. M. Z. Bulatovic, D. Maksimovic-Ivanic, C. Bensing, S. Gomez-Ruiz, D. Steinborn, H. Schmidt, M. Mojic, A. Korac, I. Golic, D.

Perez-Quintanilla, M. Momcilovic, S. Mijatovic and G. N. Kaluderovic, *Angew. Chem.-Int. Edit.*, 2014, 53, 5982-5987.
52. L. Z. He, Y. Y. Huang, H. L. Zhu, G. H. Pang, W. J. Zheng, Y. S. Wong and T. F. Chen, *Adv. Funct. Mater.*, 2014, 24, 2754-2763.
53. J. Shen, G. S. Song, M. An, X. Q. Li, N. Wu, K. C. Ruan, J. Q. Hu and R. G. Hu, *Biomaterials*, 2014, 35, 316-326.
54. F. Muhammad, W. Qi, A. Wang, J. Gu, J. Du and G. Zhu, *Journal of Materials Chemistry B*, 2015, 3, 1597-1604.
55. Y. Zhang, Z. Hu, G. Xu, C. Gao, R. a. Wu and H. Zou, *Nano Research*, 2014, 7, 1103-1115.
56. L. He, H. Lai and T. Chen, *Biomaterials*, 2015, 51, 30-42.
57. N. Hao, H. Yang, L. Li, L. Li and F. Tang, *New Journal of Chemistry*, 2014, 38, 4258-4266.
58. L. Zeng, J. Chen, S. Ji, L. Chan, W. Zheng and T. Chen, *Journal of Materials Chemistry B*, 2015, 3, 4345-4354.
59. B. Hou, B. Zheng, X. Gong, H. Wang, S. Wang, Z. Liao, X. Li, X. Zhang and J. Chang, *Journal of Materials Chemistry B*, 2015, 3, 3531-3540.
60. H. Zheng, C. Gao, B. Peng, M. Shu and S. Che, *The Journal of Physical Chemistry C*, 2011, 115, 7230-7237.
61. C.-H. Lee, L.-W. Lo, C.-Y. Mou and C.-S. Yang, *Advanced Functional Materials*, 2008, 18, 3283-3292.
62. F. Lu, S.-H. Wu, Y. Hung and C.-Y. Mou, *Small*, 2009, 5, 1408-1413.
63. J. G. Haasnoot, *Coordination Chemistry Reviews*, 2000, 200–202, 131-185.
64. J.-P. Zhang, Y.-Y. Lin, X.-C. Huang and X.-M. Chen, *Journal of the American Chemical Society*, 2005, 127, 5495-5506.
65. S. Velu, L. Wang, M. Okazaki, K. Suzuki and S. Tomura, *Microporous and Mesoporous Materials*, 2002, 54, 113-126.
66. H. W. Luo, J. J. Chen, G. P. Sheng, J. H. Su, S. Q. Wei and H. Q. Yu, *Scientific reports*, 2014, 4, 7078.
67. H. Q. Zheng, L. Xing, Y. Y. Cao and S. A. Che, *Coord. Chem. Rev.*, 2013, 257, 1933-1944.
68. B. Pauwels, A. E. C. Korst, C. M. J. de Pooter, G. G. O. Pattyn, H. A. J. Lambrechts, M. F. D. Baay, F. Lardon and J. B. Vermorken, *Cancer Chemotherapy and Pharmacology*, 2003, 51, 221-226.
69. M. M. Stevanovic, S. D. Skapin, I. Bracko, M. Milenkovic, J. Petkovic, M. Filipic and D. P. Uskokovic, *Polymer*, 2012, 53, 2818-2828.
70. R. R. Tice, E. Agurell, D. Anderson, B. Burlinson, A. Hartmann, H. Kobayashi, Y. Miyamae, E. Rojas, J. C. Ryu and Y. F. Sasaki, *Environ. Mol. Mutagen.*, 2000, 35, 206-221.
71. L. M. Milchak and J. D. Bricker, *Toxicol. Lett.*, 2002, 126, 169-177.
72. B. A. Wagner, C. B. Evig, K. J. Reszka, G. R. Buettner and C. P. Burns, *Arch. Biochem. Biophys.*, 2005, 440, 181-190.
73. J. Dai, R. S. Weinberg, S. Waxman and Y. K. Jing, *Blood*, 1999, 93, 268-277.
74. J. D. Ly, D. R. Grubb and A. Lawen, *Apoptosis*, 2003, 8, 115-128.
75. N. Zamzami and G. Kroemer, *Curr. Biol.*, 2003, 13, R71-R73.